CrossMark

ORIGINAL ARTICLE

Biologically produced silver chloride nanoparticles from *B. megaterium* modulate interleukin secretion by human adipose stem cell spheroids

Letícia E. Charelli · Nathalia Müller · Karina R. Silva · Luís Maurício T. R. Lima · Celso Sant'Anna · Leandra S. Baptista

Abstract Stem cell tissue constructs are likely to come into contact with silver-based nanoparticles—such as silver chloride nanoparticles (AgCl–NPs)—used as microbicidals at the implant site or in cosmetics. However, the effect of silver-based nanoparticles on 3D cell cultures with potential for tissue engineering has received little attention. Here, we examined the effect of sub-lethal doses (5, 10 and 25 μg/mL, for 1, 7 and 21 days) of AgCl–NPs produced by 'green' bacterial-based synthesis on spheroid 3D cultures of human adipose tissue stem cells (ASCs). Light microscopy analysis revealed that the shape and diameter of ASC spheroids remained largely unchanged after AgCl–NP treatment. Flow cytometry analysis with 7-AAD and 2′,7′-dichlorofluorescein diacetate revealed no statistically significant differences in cell death but showed an increase of ROS levels for the untreated group and significant differences for the groups treated with 5 and 10 μg/mL at day 7 ($p = 0.0395$, $p = 0.0266$, respectively). Electron microscopy analysis showed limited cell damage in the periphery of AgCl–NP-treated spheroids. However, treatment with AgCl–NP had statistically

Letícia E. Charelli and Nathalia Müller have contributed equally to this work.

L. E. Charelli · N. Müller · K. R. Silva ·
C. Sant'Anna · L. S. Baptista
Post-graduation Program in Biotechnology, National Institute of Metrology, Quality and Technology (Inmetro), Duque de Caxias, Rio de Janeiro, Brazil

L. E. Charelli · K. R. Silva · L. S. Baptista
Laboratory of Tissue Bioengineering, National Institute of Metrology, Quality and Technology (Inmetro), Duque de Caxias, Rio de Janeiro, Brazil

L. E. Charelli · K. R. Silva · L. S. Baptista (✉)
Nucleus of Multidisciplinary Research in Biology (Numpex-Bio), Federal University of Rio de Janeiro-Xerém (UFRJ – Xerém), Duque de Caxias, Rio de Janeiro, Brazil
e-mail: leandrabaptista@xerem.ufrj.br

N. Müller · C. Sant'Anna
Laboratory of Microscopy Applied to Life Science (Lamav), National Institute of Metrology, Quality and Technology (Inmetro), Duque de Caxias, Brazil

L. M. T. R. Lima
Laboratory of Pharmaceutical Biotechnology, Federal University of Rio de Janeiro (UFRJ), Rio de Janeiro, Brazil

significant effects on the secretion of IL-6, IL-8, IL-1β and IL-10 by spheroids, at specific treatment periods and concentrations, and particularly for IL-6, IL-8 and IL-1β. TGF-β1 and -β2 secretion also changed significantly throughout the treatment period. Our results indicate that, despite having little effect on cell viability and morphology, sub-lethal AgCL–NP doses modulate ROS production at day 7 for the groups treated with 5 and 10 μg/mL and also modulate the secretory profile of ASC spheroids. Thus, the use of skin implants or products containing Ag-NPs may promote long-term disturbances in subcutaneous adipose tissue homeostasis.

Keywords Spheroids · Silver chloride nanoparticles · Adipose stem cells · 3D culture · Interleukin secretion

Introduction

Human exposure to nanoparticles has increased in the last decade mostly due to the emergence of the rapidly developing field of nanotechnology. Silver-based nanoparticles, especially metallic silver nanoparticles, are the most extensively explored nanoparticle type in the industrial sector (Adnan and Kang 2015). Both metallic silver nanoparticles (AgNPs) and silver chloride nanoparticles (AgCl–NPs) have well-known antimicrobial and antiseptic properties (Ferreira et al. 2017; Acharya et al. 2018). Thus, these nanoparticles have been widely incorporated into several household and biomedical products such as implants, catheters, clothes, cosmetics, food items and medicinal products (e.g., hydrogels for burn treatment). The microbicidal effect of nanoparticles is due to blockage of microbial DNA replication, respiratory enzyme pathway activity and cell wall formation (Jung et al. 2008; Wijnhoven et al. 2009).

Currently, silver-based nanoparticles can be produced by chemical, physical, and biological methods (Barkat et al. 2017). The biological (or 'green') route makes use of microorganisms and plants for the reduction of silver ions, and has been considered a simple and viable alternative to the chemical and physical methods, which have adverse effects associated with the use of biologically hazardous chemicals, aside from high operational costs and energy needs

(Zhang et al. 2016b). The microbial sources for the production of silver-based nanoparticles include prokaryotes and eukaryotes, such as bacteria, fungi and microalgae (Srikar et al. 2016). Silver is highly toxic to most microbes, and the synthesis of silver nanoparticles by microorganisms may represent a defensive mechanism for silver detoxification, by converting reactive silver ions into stable silver atoms (Tripathi et al. 2017).

Previous studies have shown that AgNPs are considerably toxic to a variety of human/mammalian cell lines, including skin (Samberg et al. 2010), brain (Luther et al. 2011), germinative (Taylor et al. 2015), liver (Park et al. 2010) and kidney cells (Gopinath et al. 2010), and also to human osteoarthritic chondrocytes (Pascarelli et al. 2013). In contrast, Qin et al. (2014) reported that AgNPs stimulate osteogenic differentiation of urine-derived stem cells at appropriate concentrations. The effects of AgNPs are beginning to be elucidated and seem to be related with oxidative cell damage, inflammatory responses, decrease in cell viability and disturbance of cells secretory profile. These effects will depend on AgNPs concentration, size/shape and surface area, and on the target cell type (Antony et al. 2015; Zhang et al. 2016a). On the other hand, the consequences of AgCl–NPs exposure in mammals need to be explored.

Human mesenchymal stem cells (hMSC), such as adipose tissue stem cells, play a major role in tissue regeneration and in the secretion of anti-inflammatory molecules at the injury site (Sart et al. 2014). These cells are widely used in tissue engineering (Waters et al. 2017; Asl et al. 2017). Due to their antimicrobial properties, silver-based nanoparticles have been used as coating in scaffolds seeded with hMSC, for tissue engineering (Chaudhury et al. 2014). Also, at skin implant sites, stem cells from subcutaneous adipose tissue found near the implant surface might be exposed to nanoparticles from the implant itself or from sunscreens and cosmetics, leading to chronic adipose stem cell exposure to nanoparticles at sub-lethal levels (Wang et al. 2009, 2016).

MSCs cultivated in three-dimensional (3D) culture systems have increased stem-cell multipotency, anti-inflammatory and proangiogenic properties compared with those grown in 2D culture (Laschke and Menger 2017; Costa et al. 2017). Cell–matrix interactions in 3D cultures create biological barriers, which generate diffusion and transport conditions more similar to

those found in vivo. Thus, the use of 3D cell culture in toxicity assays may increase the accuracy of in vitro drug testing, by providing assay conditions closer to those found in vivo. Our laboratory has shown that human stem cells derived from adipose tissue (adipose stem cells, or ASCs) form spheroids in vitro under appropriate conditions, and have significant potential in tissue engineering (Stuart et al. 2017). Despite the potential of ASC 3D cultures for use in tissue engineering and toxicity analyses, the response of ASCs to AgCl–NPs in spheroid 3D cultures has not been examined.

Although the cellular effects of treatment with silver-based nanoparticles at cytotoxic levels have been well studied, little is known about the response of cells to sub-lethal doses of these nanoparticles, which are most likely to occur in vivo. In the present study, we evaluated if the exposure of spheroid 3D cultures made from human ASCs to sublethal AgCl–NPs concentrations would affect the secretion of immunomodulatory and repair molecules, including interleukins and transforming growth factor-β (TGF-β) isoforms.

Materials and methods

Biosynthesis and purification of silver chloride nanoparticles

Bacillus megaterium ATCC 14581 was cultivated in nutrient broth media (1% peptone, 0.5% beef extract and 0.5% yeast extract) (Himedia, Mumbai, India) for 24 h, at 30 °C. Then, an aqueous solution of 3.5 M $AgNO_3$ (Merck, Rio de Janeiro, Brazil) was added to the cultures for a final concentration of 3.5 mM, and cultures were maintained for 7 days in the dark at 37 °C, and under agitation at 150 rpm.

The synthesis of silver-based nanoparticles was monitored visually by medium color change, and confirmed by UV–visible spectroscopy using a Spectra Max 190 spectrophotometer, in the spectrum range from 300 to 700 nm, with 1 nm increments.

Cultures containing nanoparticles were centrifuged at $2720 \times g$ for 10 min at room temperature, to separate silver-based nanoparticles from the cell pellet. After that, nanoparticles were washed 3 times in 2% sodium citrate solution (pH 8.0), isolated by centrifugation at $38,360 \times g$ for 20 min, and then resuspended in 2% sodium citrate solution (pH 8.0). Nanoparticle solutions were kept at 4 °C until further use.

Energy dispersive X-ray spectroscopy (EDS) analysis of nanoparticles

Purified nanoparticles were dried at 60 °C for 40 min and the dried powder was adhered onto scanning electron microscopy (SEM) stubs coated with carbon tape. Samples were observed in a FEI Quanta FEG 450 Scanning Electron Microscope (FEI, Eindhoven, Netherlands), equipped with an EDS unit, and operating at 5 kV. The Genesis software (from the EDAX EDS System) was used to identify the elements present in the sample.

X-ray diffraction (XRD)

Purified nanoparticles were dried at 60 °C for 40 min, mounted onto 10 µm nylon loops (Hampton Research, Aliso Viejo, CA, USA) and subjected to diffraction with radiation of 1.5416 Å (CuKa) in the angular range of 20–80 (2θ angles), using a SuperNova diffractometer equipped with a Titan CCD detector (Agilent, Santa Clara, CA, USA), and operating at 40 W (50 kV and 0.5 mA). Samples were exposed for 300 s, and measurements were corrected for dark noise subtraction under similar conditions. The baseline was corrected using the FityK program (http://fityk.nieto.pl/), and the XDR spectra were further analyzed by deconvolution based on a Gaussian distribution for each energy peak. The diffraction profile was compared with that of silver chloride nanoparticles published by the Joint Committee on Powder Diffraction standards (JCPDS: 31-1238).

Morphometric analysis by transmission electron microscopy (TEM)

To determine the size and circularity of the nanoparticles, aliquots (5 µm) of isolated AgCl–NPs in aqueous solution were deposited onto Formvar/carbon-coated copper grids (EMS, Lancaster, PA, USA), allowed to dry, and imaged in a Tecnai Spirit Biotwin G2 transmission electron microscope (FEI), operating at 120 kV. Then, nanoparticle diameter and circularity (n = 1200 particles) were measured from digital TEM images, using the ImageJ software.

Human lipoaspirate samples and adipose stem cell isolation

Human lipoaspirate samples were obtained from healthy donors (n = 2) that underwent plastic surgery. This study was approved by the Research Ethics Committee of the Clementino Fraga Filho University Hospital, Federal University of Rio de Janeiro (UFRJ, Brazil; Protocol 145-09), and informed consent was obtained from all individuals whose samples were used in the study. Tissue samples were stored at 4 °C after surgery, and stem cell isolation was performed within 18 h of sample collection. Adipose tissue samples were distributed into tubes containing ACK (red blood cell lysis) buffer solution (1:1, v/v) (Lonza, Salto, Brazil), the mixture was vortexed in 5 pulses of 1 min each, in a horizontal position. Then, samples were maintained at 37 °C for 15 min, for red blood cell lysis. Cells were separated from adipose tissue fragments, oil and debris by centrifugation at 900 g for 15 min at room temperature. Cells (in the pellet) were plated in 25 cm^2 culture flasks (at 10^5 cells/cm^2) with Chemically Defined Mesenchymal Stem Cell Medium (MSCGM-CD^{TM}-Lonza, Walkersville, MD, USA) supplemented with 2% fetal bovine serum, 100 µg/mL penicillin and 100 µg/mL streptomycin (Sigma Aldrich, St. Louis, MO, USA), and maintained at 37 °C (with 5% of CO_2). The medium was changed every 3 days until the cell monolayer reached confluence, as previously described by our research group (Baptista et al. 2009).

Spheroid formation

ASCs from confluent monolayers were harvested using 0.125% trypsin and 0.78 mM ethylenediamine tetraacetic acid (EDTA) (both from Gibco-BRL, Gaithersburg, MD, USA). Cell suspensions were centrifuged at 400g for 5 min, and 2 × 10^6 cells in DMEM (supplemented as described below) were plated into micro-molded non-adhesive hydrogel with 81 circular recesses (2% agarose—UltrapureAgarose, Invitrogen, Waltham, MA, USA—in 0.9% NaCl), according to the manufacturer's recommendations (Microtissue Inc., USA), and incubated for 24 h, at 37 °C (and 5% of CO_2), for the formation of one spheroid in each circular recess. Spheroid 3D cultures were maintained in DMEM supplemented with 50 µg/mL ascorbic acid (Sigma), 1.25 µg/mL human albumin (Farma Biagini SPA, Castelvecchio Pascoli,

Italy), 100 µg/mL penicillin, 100 µg/mL streptomycin (Sigma) and Insulin-Transferrin-Selenium (ITS) (1 ×; Lonza) at 37 °C (and 5% of CO_2), for 3 days prior to use in AgCl–NP treatment assays.

Treatment with AgCl–NPs

ASC spheroids were treated with sub-lethal concentrations of AgCl–NPs (5, 10 and 25 µg/mL, prepared from stock solutions at 175 µg/mL) for 1, 7 and 21 days, in the original hydrogel, and in DMEM supplemented as described above, at 37 °C (and 5% CO_2). The morphology of ASC spheroids was also examined by phase contrast microscopy, in an inverted microscope (Carl Zeiss MicroImaging GmbH, Göttingen, Germany). Cell diameter measurements were produced from light microscopy images (using the AxioVision LE64 software) of 4 spheroids in two independent experiments.

Flow cytometry

ASC spheroids were harvested from the hydrogel at days 1, 7 and 21 post-treatment, and dissociated with 1 mg/mL collagenase type IA, at 37 °C for 30 min. After dissociation, cell suspensions were centrifuged at 900g for 15 min and resuspended in PBS. For cell viability analysis, cells were incubated with a monoclonal antibody anti-CD90-allophycocyanin (Cat. no. 555596; BD Biosciences, San Jose, CA, USA) and then labeled with the DNA intercalant 7AAD (BD Biosciences). To quantify reactive oxygen species (ROS), cells were labeled with 2′,7′-dichlorofluorescein diacetate (Sigma). All staining procedures were performed according to manufacturers' recommendations. Two independent experiments were performed and 20,000 events were acquired in a FACSAria III equipped with the FACSDiva 8.0 software (BD Biosciences). The percentage of viable and ROS positive cells was determined among CD90 positive cells.

Scanning electron microscopy (SEM) and energy-dispersive X-ray spectroscopy (EDS) of nanoparticle treated ASC spheroids

ASC spheroids (untreated or treated with 10 µg/mL AgCl–NPs for 7 days) were fixed in 2.5% glutaraldehyde, 4% paraformaldehyde in 0.1 M cacodylate buffer (pH 7.3) for 30 min, and post-fixed in 1% osmium

tetroxide/0.8% potassium ferrocyanide/5 mM calcium chloride, in 0.1 M cacodylate buffer, for 30 min (protected from light). After washes in 0.1 M cacodylate buffer, samples were dehydrated in a series of ethanol solutions (30, 50, 70, 90 and 100%, for 30 min in each concentration), critical point-dried in a Leica EM CPD 030 apparatus, and mounted onto carbon tape-coated SEM stubs (EMS). Samples were sputter coated with a 2–3-nm-thick titanium layer using a Leica EM SCD 500 sputtering device (Wetzlar, Germany). Secondary (SEI) and backscattered (BSE) electron images were obtained in a Quanta FEG 450 scanning electron microscope, at an accelerating voltage of 5.0 kV.

For EDS analysis, samples were allowed to adhere onto carbon conductive tape previously attached to SEM stubs and observed in a Quanta FEG 450 scanning electron microscope, equipped with an EDS unit, and operating at 20 kV. The EDAX EDS system and Genesis software were used to identify the elements present in the sample.

Ultrathin section transmission electron microscopy (TEM)

ASC spheroids (untreated or treated with 10 μg/mL AgCl–NPs for 7 days) were fixed and post-fixed as described above (for SEM and EDS), dehydrated in an acetone series (50, 70, 90 and 100%) and embedded in PolyBed 812 resin. Ultrathin sections obtained using a Leica EM UC ultramicrotome were stained with uranyl acetate and Reynolds' lead citrate and observed in a FEI Tecnai Spirit Biotwin G2 TEM, operating at 80 kV.

Quantification of interleukins and TGF-β isoforms in culture supernatants

The culture medium of ASC spheroids treated as described above (see "Treatment with AgCl–NPs") was changed to fresh medium lacking AgCl–NPs, and spheroids were incubated for 24 h at 37 °C (and 5% CO_2). Then, culture supernatants were collected and frozen at − 80 °C. Immediately prior to analysis, samples were thawed on ice (for TGF-β1, -β2 and -β3 analyses only, samples were transferred to − 20 °C 24 h before this step) and prepared according to the manufacturers' recommendations. For the quantification of IL-8, IL-1β, IL-6 and IL-10, the BD[TM] Cytometric Bead Array (CBA) flex set assays was used. IL-10, IL-1β and TNF quantification was

performed using the BD[TM] Cytometric Bead Array (CBA) enhanced sensitivity flex set assays. A multiplex immunoassay (BioPlex MAGPIX assay kit, from BioRad Laboratories, Hercules, CA, USA) was performed to quantify TGF-β1, -β2 and -β3 levels in culture supernatants. CBA data were acquired in a FACSAria III equipped with the software FACS Diva 8.0 (BD Biosciences), and analyzed using FCAP Array software version 3.0. Luminex immunoassay plates were read in a BioPlex MAGPIX equipment and data were analyzed by the xPONENT software version 4.2. The concentration of each analyte was quantified in culture supernatants of ASCs spheroids using three technical replicates of two independent experiments.

Statistical analysis

Comparisons among untreated and AgCl–NP-treated samples were performed using one-way analysis of variance (ANOVA) test followed by post hoc test. Differences were considered statistically significant if $p < 0.05$. Statistical analyses were performed using the software GraphPad Prism 6.0 (GraphPad Software, La Jolla, CA, USA).

Results

Bacillus megaterium cultures synthesize AgCl–NPs

Stem cell-based implants may come into contact with silver-based nanoparticles, which are used as microbicidal agents in health care and cosmetic products. We treated 3D cultures of ASC spheroids with sublethal doses of silver chloride nanoparticles, to mimic more closely the conditions of exposure of stem cell implants to these particles. The nanoparticles used here were bioproduced from cultures of the Gram-positive bacterium *B. megaterium*, after incubation with 3.5 mM $AgNO_3$ for 7 days (Fig. 1a). The growth medium color change from pale yellow to dark brown indicating nanoparticle biosynthesis (Fig. 1a, inset), which was confirmed by UV–Vis analysis showing absorbance in the spectrum range of 380–450 nm, with maximum absorbance at 416 nm (Fig. 1a).

Energy dispersive X-ray (EDS) spectroscopy analysis of the powder of purified nanoparticles (Fig. 1b) showed peaks at 3 keV and 2.75 keV, corresponding
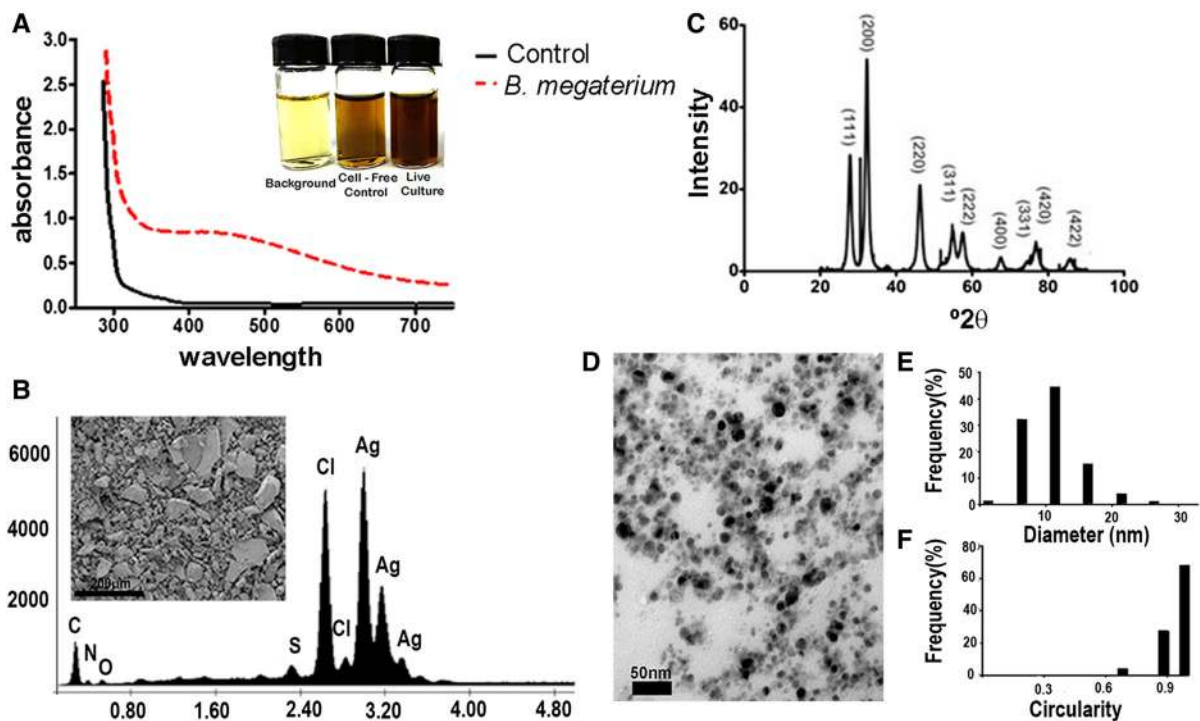
Fig. 1 Characterization of silver chloride nanoparticles (AgCl–NPs) produced by *Bacilllus megaterium* cultures. **a** UV–Vis spectrum (300–700 nm) of the culture medium (background, black line) and of a *B. megaterium* culture (dotted red line) after 7 days of incubation with 3.5 mM AgNO₃ at 37 °C. a. u., arbitrary units. (**a**, inset) Image of glass vials containing growth medium with no AgNO₃ ("Background"), growth medium containing AgNO₃ and incubated for 5 days without a bacterial inoculum ("Cell-free control") and a *B. megaterium* culture incubated with AgNO₃ for 5 days ("Live culture"). **b** Energy dispersive X-ray spectroscopy (EDS) analysis of the purified nanoparticles (in the powder form) from *B. megaterium*

cultures. a. u., arbitrary units. (**b**, inset) Scanning electron microscopy (SEM) secondary electron image of the nanoparticle powder shown in (**b**). Scale bar, 200 μm. **c** X-ray diffraction (XRD) pattern of purified nanoparticles showing diffraction peaks corresponding to AgCl–NP lattice planes of 27.8° (111), 32.2° (200), 46.2° (220), 54.8° (311), 57.6° (222), 67.5° (400), 74.5° (331), 76.9° (420), and 85.7° (422). **d–f** Morphometric analyses AgCl–NP size (diameter, in **e**) and shape (circularity, in **f**), measured from 1200 particles (as in **d**; scale bar, 50 nm). Most AgCl–NPs had diameter of 5–10 nm, and a spherical morphology (i.e., circularity of 0.9–1.0). (Color figure online)

to silver and Cl⁻ atoms, respectively (Fig. 1b), suggesting that the nanoparticles produced by *B. megaterium* cultures were made of silver chloride (AgCl–NPs). The peaks of carbon, nitrogen, oxygen and sulfur also found in the EDS profile are likely to correspond to minor contaminants from the medium broth and/or from bacterial components.

The powder of purified nanoparticles from *B. megaterium* cultures was then subjected to X-ray diffraction (XRD) analysis, for accurate chemical identification (Fig. 1c). The data were compared with two standards set by the Joint Committee on Powder Diffraction standards (JCPDS file no. 85-1355), to determine the plane orientation of the particles produced. The XRD spectrum of purified

nanoparticles exhibited 9 peaks at the following 2θ values (with corresponding indexed planes in parenthesis): of 27.8° (111), 32.2° (200), 46.2° (220), 54.8° (311), 57.6° (222), 67.5° (400), 74.5° (331), 76.9° (420), and 85.7° (422). These planes correspond to those of the cubic crystalline phase of silver chloride. The diffraction profile is consistent with the JCPDS standards for silver chloride nanoparticles (AgCl–NPs) (JCPDS: 31-1238).

Morphometric analyses of 1200 individual nanoparticles by transmission electron microscopy (TEM) showed that particles ranged from 4 to 26 nm, with an average diameter of 13 ± 4 nm (Fig. 1d). Most AgCl–NPs (∼ 45%) had a diameter of ∼ 10 nm, with a smaller proportion of particles of ∼ 5 nm

and ∼ 15 nm in diameter (∼ 30% and 18%, respectively) (Fig. 1e). The circularity analysis indicated that approximately 80% of nanoparticles had a spherical morphology (Fig. 1f).

AgCl–NP treatment had only minor effects on ASC spheroid diameter, cell viability and ROS levels

We chose to test here the concentrations of 5, 10 and 25 µg/mL of AgCl–NP, which were established as sub-lethal in viability assays using AgCl–NP concentrations of 5 µg/mL up to 70 µg/mL (not shown). As an initial step to analyze the effect of AgCl–NPs on ASC spheroid cultures, we treated spheroids with 5, 10 and 25 µg/mL AgCl–NPs for 1, 7 and 21 days, and examined spheroid morphology, viability and ROS production. Light microscopy images revealed that the spheroid shape remained unaltered after treatment with AgCl–NPs, even at the highest concentrations and longest treatment periods (Fig. 2a–l). However, the spheroid diameter increased significantly after treatment with 5 µg/mL for 1 day ($p = 0.0030$), and 10 µg/mL for 7 days ($p < 0.0001$). The highest concentration of AgCl–NPs tested here did not alter the diameter of spheroids relative to the untreated control, and at day 21 the spheroids treated with 25 µg/mL had a smaller diameter (closer to that of control cells) than those treated with 10 µg/mL ($p = 0.0004$) (Fig. 2m).

Flow cytometry analysis revealed no statistically significant loss in ASC viability during the treatment period, for spheroids treated with 5, 10 and 25 µg/mL AgCl–NPs (Fig. 2n). ROS analysis by flow cytometry revealed a significant increase of ROS levels exclusively between 1 and 7 days of treatment, for both concentrations of 5 ($p = 0.0395$) and 10 µg/mL ($p = 0.0266$) (Fig. 2o).

AgCl–NPs did not alter the ultrastructure of ASC spheroids

To assess the effect of a sub-lethal dose of AgCl–NPs on spheroid morphology, we examined spheroids treated with 10 µg/mL AgCl–NPs for 7 days by both scanning (SEM; Fig. 3a–c) and transmission (TEM; Fig. 3d–f) electron microscopy. Secondary electron image (SEI) views by SEM showed that there were no obvious ultrastructural changes in the spheroid surface after treatment with AgCl–NPs, compared with untreated spheroids (Fig. 3a, d). Backscattered electron (BSE) images by SEM confirmed the presence of bright dots likely corresponding to AgCl–NPs (arrows, in Fig. 3b) adhered to the surface of treated spheroids. Silver EDS peaks collected from these bright dots confirmed that they corresponded to AgCl–NPs (Fig. 3b, inset). The TEM analysis showed that the loss of cellular integrity in treated samples was restricted to a few cells located in the peripheral layer of the treated spheroids (Fig. 3e, f, asterisks). Below this layer both the pattern of cellular arrangement and the cell ultrastructure appeared undisturbed (Fig. 3e). A detailed image comparison showed that the ultrastructure of key cytoplasmic elements (such as the nucleus, mitochondria and lipid bodies) of cells in the interior of treated spheroids (Fig. 3e) was indistinguishable from that of internal cells from untreated spheroids (Fig. 3d).

AgCl–NPs altered the pattern of interleukin secretion by ASC spheroids and the secretion of TGF-β isoforms

Given the importance of paracrine signaling for stem cell populations at the implantation site, we compared the levels of specific molecules in the supernatant of treated and untreated ASC spheroids. We observed detectable levels of the pro-inflammatory interleukins IL-6, IL-1β and IL-8 (Fig. 4a–c), and of the anti-inflammatory interleukin IL-10 (Fig. 4d), in the supernatant of treated ASC spheroids throughout the period of treatment with AgCl–NPs.

IL-6 levels at day 1 were dose-dependent increased for all treated ASC spheroids compared with untreated spheroids ($p < 0.0001$). Furthermore, treated ASC spheroids showed a dose-dependent increase of IL-6 levels throughout the treatment period ($p = 0.0009$). Curiously, at day 21 treated ASC spheroids with 25 µg/mL showed the highest level of IL-6 throughout the treatment period. This increase was significant compared with untreated and treated ASC spheroids with 5 and 10 µg/mL groups ($p < 0.0001$) and compared with the same treated ASC spheroids (25 µg/mL) in early days of treatment ($p < 0.0001$) (Fig. 4a).

IL-8 levels also showed a dose-dependent increase for all treated ASC spheroids throughout the treatment period ($p < 0.0001$). At day 7 IL-8 levels significantly decreased in all treated ASC spheroids compared with untreated spheroids ($p < 0.0001$). At day 21, treated
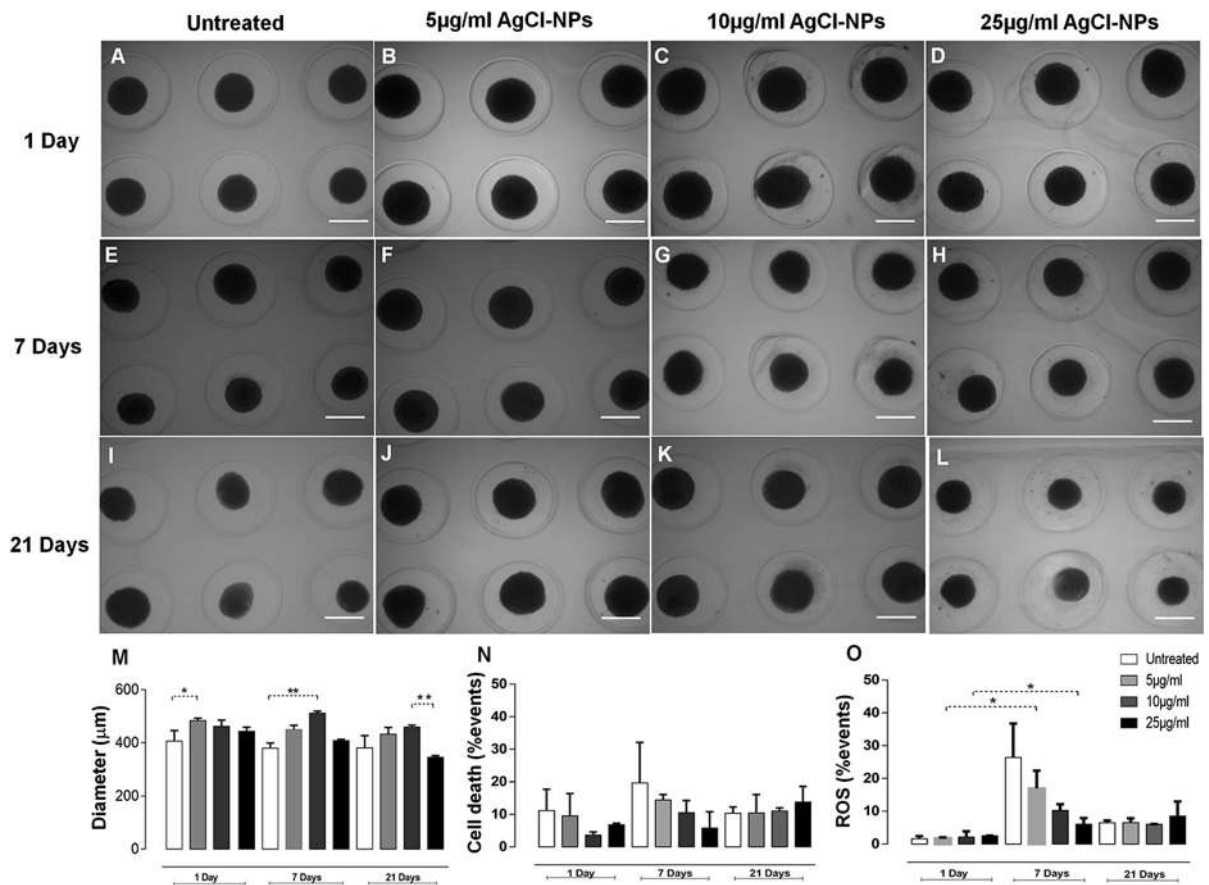
Fig. 2 Light microscopy, cell death and ROS analyses of adipose stem cell (ASC) spheroids. ASC spheroids were treated with different concentrations of AgCl–NPs (5, 10 and 25 μg/mL) for 1, 7 or 21 days, and then examined by light microscopy (**a–m**), or subjected to dissociation for flow cytometry assays to quantify cell death (**n**) and reactive oxygen species (ROS) levels (**o**). **a–l** Phase contrast microscopy images of treated and untreated spheroids in micromolded agarose. Scale bar: 400 μm. **m** Morphometric analysis of spheroid diameter, based on images such as those shown in **a–l**. Each experimental group corresponds to the mean ± SD of four spheroids from two independent experiments. $*p < 0.05$, $**p < 0.001$ (by ANOVA with Kruskal–Wallis post hoc test). **n** The percentage of cell death, quantified by positive staining with the DNA intercalating dye 7AAD. No statistically significant differences between samples were observed by ANOVA with Tukey's post hoc test. **o** Quantification of cells with increased ROS levels, as identified by positive staining with 2′,7′-dichlorofluorescin diacetate. Asterisk represents the result of Tukey's post hoc test ($*p < 0.05$). **n**, **o** Each experimental group corresponds to the mean ± SD of two independent experiments through which 20,000 events were evaluated

ASC spheroids with 10 μg/mL showed highest levels of IL-8 compared with 5 μg/mL and 25 μg/mL treated spheroids ($p = 0.0017$). On the contrary of IL-6 levels at day 21, ASC spheroids treated with 25 μg/mL at day 21 showed a significant decrease of IL-8 levels compared with untreated spheroids ($p = 0.0017$). Curiously, ASC spheroids treated with 10 μg/mL showed a significant increase of IL-8 levels throughout the treatment period ($p = 0.0003$) (Fig. 4b).

IL-1β was not detected at day 1 of AgCl–NP treatment. At day 7, IL-1β levels were detected exclusively in the supernatant of ASC spheroids treated with 25 μg/mL, showing statistical significance compared with 5 and 10 μg/mL treated ASC spheroids ($p = 0.0030$). IL-1β levels at day 21 for ASC spheroids treated with 25 μg/mL showed a significant increase compared with 5 and 10 μg/mL treated ASC spheroids ($p = 0.0035$) (Fig. 4C).

IL-10 was not detected at day 1 of AgCl–NP treatment. At day, 7 IL-10 levels for ASCs spheroids treated with 5 μg/mL were significantly highest compared with untreated spheroids ($p = 0.0251$).
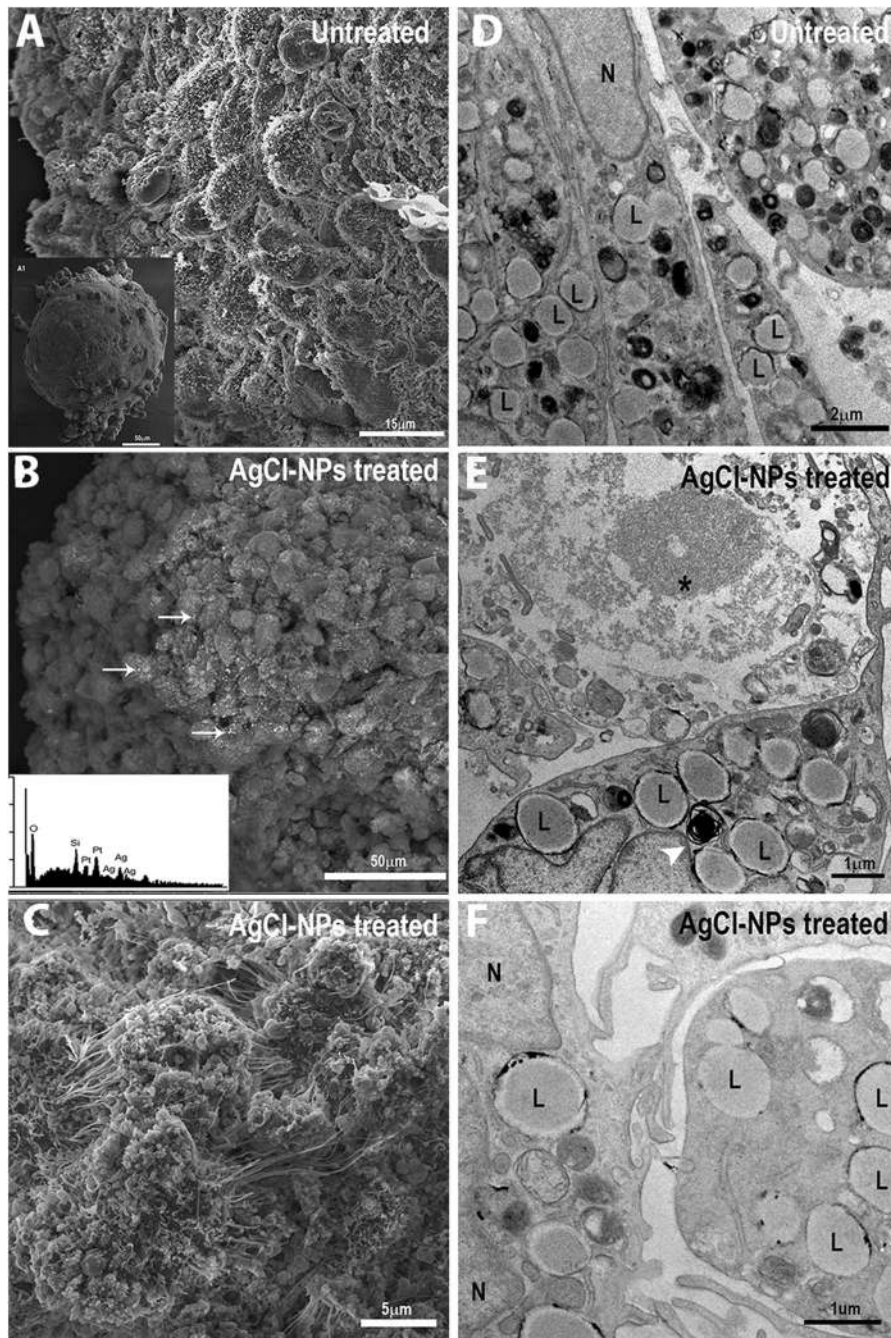
Fig. 3 Electron microscopy analysis of adipose stem cell (ASC) spheroids after treatment with silver chloride nanoparticles (AgCl–NPs). The morphology of ASC spheroids was assessed by scanning (SEM; **a–c**) and transmission (TEM; **d–f**) electron microscopy. **a**, **d** Untreated ASC spheroids. **b**, **c**, **e**, **f** Spheroids treated with 10 μg/mL of AgCl–NPs for 7 days. **b** No obvious ultrastructural changes in the spheroid surface were found after AgCl–NPs treatment. White arrows indicate the presence of AgCl–NPs on the spheroid surface, which was confirmed by energy dispersive X-ray (EDS) analysis (insert). **c** Higher-magnification image of the surface of a spheroid in which no structural changes were seen. **e** TEM image of a treated ASC spheroid, showing a damaged cell on the spheroid surface (asterisk) The arrowhead indicates a myelin corpuscle. **f** TEM image of a treated ASC spheroid, showing another area of cells on the spheroid surface with disrupted interaction. L: lipid vacuole. N: nucleus. Scale bars: **a** 15 μm; **b** 50 μm; **c** 5 μm; **d** 2 μm; **e**, **f** 1 μm
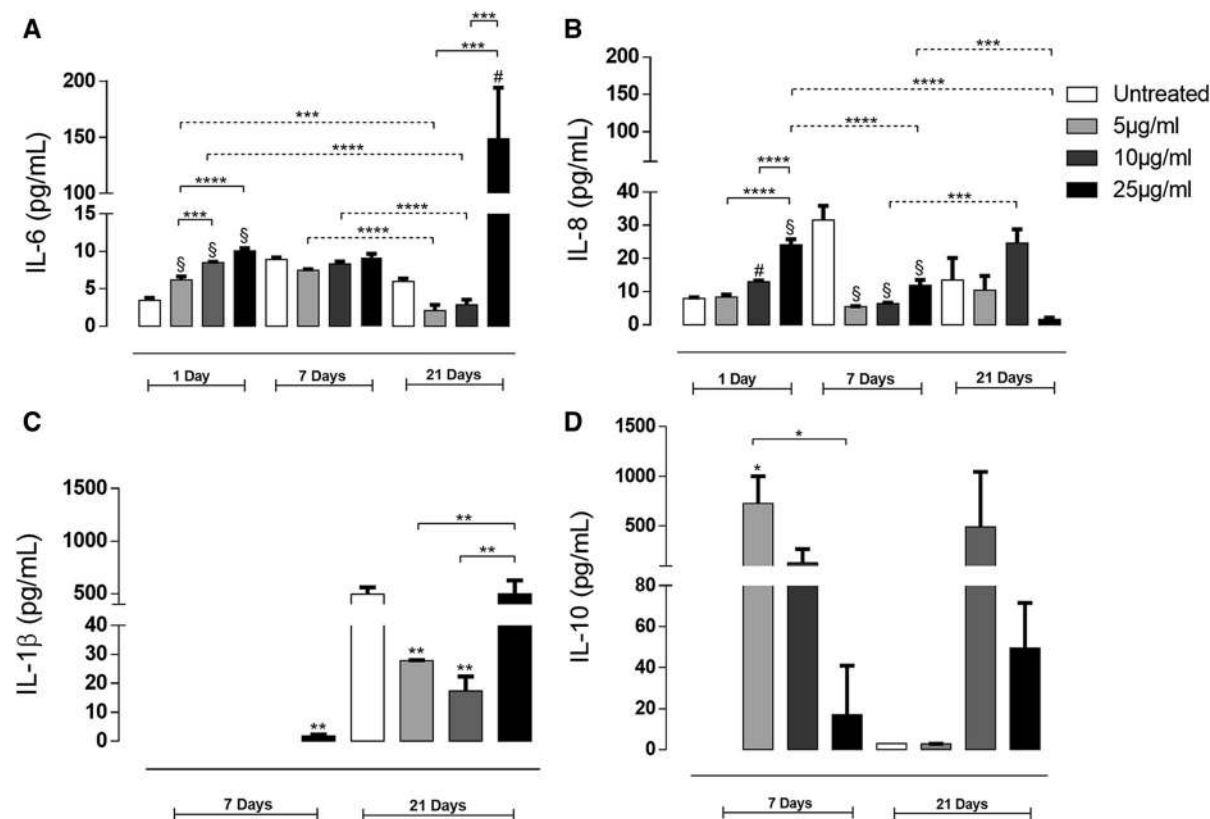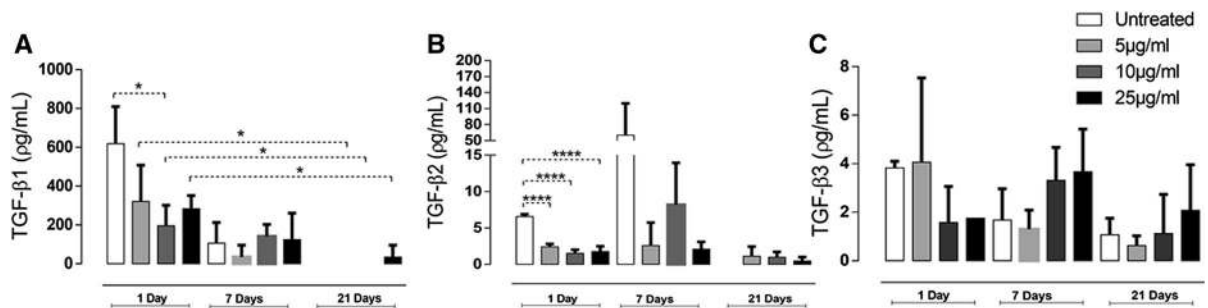
Fig. 4 Interleukin levels in adipose stem cell (ASC) spheroid cultures treated with silver chloride nanoparticles (AgCl–NPs). ASC spheroids were treated with different concentrations of AgCl–NPs (5, 10 and 25 μg/mL) for 1, 7 or 21 days, and then the levels of IL-6 (**a**), IL-8 (**b**), IL-1β (**c**) and IL-10 (**d**) were measured in spheroid culture supernatants, using cytometric bead arrays (CBA). Each experimental group corresponds to two independent experiments with three technical replicates. Results are expressed as mean ± SD. § Represents the result of Tukey's post hoc test when ANOVA test resulted a p value < 0.0001 for the comparison between the untreated

and treated groups. #Represents the result of Tukey's post hoc test when ANOVA test resulted a p value $p = 0.001$ for the comparison between the untreated and treated groups. Dotted lines represent the differences among the days of treatment (*p value ***$p = 0.001$, ****$p < 0.0001$ by Tukey's post hoc test). Solid lines represent the differences among the groups treated with different doses of AgCl–NPs (*$p < 0.05$, **$p = 0.01$, ***$p = 0.001$, ****$p < 0.0001$ by Tukey's post hoc test). Results of Tukey's post hoc test when ANOVA test resulted a p value ≥ 0.001 and < 0.05 were omitted to improve graphics visualization

Curiously, ASC spheroids treated with 25 μg/mL at day 7 showed low levels of IL-10 with statistical significance compared with 5 μg/mL treated ASC spheroids ($p = 0.0251$) (Fig. 4d).

We also quantified of TGF-β1, -β2 and -β3 levels in culture supernatants after 1, 7 and 21 days of treatment of ASC spheroids with AgCl–NPs (Fig. 5). TGF-β1 levels in all conditions (treated and untreated) were high at day 1 compared with day 7. The levels of TGF-β1 continued to decrease and at day 21, TGF-β1 was only detectable in the supernatant of spheroids treated with 25 μg/mL. TGF-β1 levels were significantly higher for all ASC spheroids treated with 5 μg/mL

($p = 0.0260$), 10 μg/mL ($p = 0.0351$) and 25 μg/mL ($p = 0.0465$) at day 1, compared with day 21 of treatment (Fig. 5A). TGF-β2 levels at day 1 showed a significant decreased for ASC spheroids treated with 5 μg/mL, 10 μg/mL and 25 μg/mL compared with untreated spheroids ($p < 0.0001$) (Fig. 5b). TGF-β3 levels did not vary significantly among treated samples, throughout the treatment period (Fig. 5c).

Fig. 5 TGF-β1, -β2 and -β3 levels in adipose stem cell (ASC) spheroid cultures treated with silver chloride nanoparticles (AgCl–NPs). ASC spheroids were treated with different concentrations of AgCl–NPs (5, 10 and 25 μg/mL) for 1, 7 or 21 days, and then the levels of TGF-β1 (**a**), -β2 (**b**) and -β3 (**c**) were measured in spheroid culture supernatants, using a multiplex immunoassay. Each experimental group corresponds to two independent experiments with three technical replicates. Results are expressed as mean ± SD. Asterisks represent the result of ANOVA with Tukey's post hoc test (*$p < 0.05$, **$p = 0.01$, ***$p = 0.001$, ****$p < 0.0001$)

Discussion

Silver-based nanoparticles are used as microbicidals in industry—in household, cosmetic and healthcare products—and may come into contact with stem-cell based implants, at sub-lethal concentrations. Although the cellular effects of silver-based nanoparticle treatment at cytotoxic levels have been well studied, little is known about the response of human cells to sublethal doses of these particles, particularly for 3D cultures. Here, we provide data indicating that sublethal concentrations of AgCl–NPs from *B. megaterium* altered the interleukin secretion profile of ASC spheroids 3D cultures.

In this work, we used purified 'green' AgCl–NPs produced by cultures of the bacterium *B. megaterium*, not previously shown to be capable of nanoparticle production. Distinct microbial species produce silver nanoparticles with different properties that affect their potential for biomedical application. The sub-lethal concentrations of nanoparticles produced by *B. megaterium* had only minor effects on the viability and shape and ROS production of ASC spheroids. Regarding the large increase in ROS production observed for the untreated group at day 7, to the best of our knowledge, there are no support in the literature for this occurrence. Regarding ASC biology, there are studies linking differentiation capacity to ROS levels (Zhang et al. 2013; Tormos et al. 2011), but nothing regarding nanoparticles exposure.

The minor effect of the nanoparticles at sub-lethal concentrations was further confirmed by electron microscopy analysis, which showed that treatment with AgCl–NPs from *B. megaterium* caused structural damage only to a few cells at the periphery of ASC spheroids. In contrast, other studies showed that treatment with AgNPs was cytotoxic to different mammalian cell lineages, including MSCs (Hackenberg et al. 2011; Alberts et al. 2011). Silver-based nanoparticle doses in the range of those tested here resulted in no cell death in mammalian cell lineages grown in 2D cultures (i.e., in monolayers), including vascular smooth muscle cells (5 μg/mL) (Hsin et al. 2008), a mouse spermatogonial stem cell line (10 μg/mL) (Stolle et al. 2005) and alveolar macrophages (25 μg/mL) (Carlson et al. 2008). The differences between our data and those reported in 2D culture studies may result from the tissue-like properties of 3D cultures. The ASC spheroid 3D culture model established in our laboratory (Stuart et al. 2017) is expected to have drug diffusion and transport conditions more similar to those observed in tissues in vivo, resulting in more physiological responses to treatment than those obtained with 2D cultures (Edmondson et al. 2014). In agreement with this notion, Lee et al. (2009) reported that gold nanoparticles were toxic to human hepatocarcinoma (HepG2) in 2D culture, but not to spheroids of these cells, possibly due to the dense cell–cell interaction and extracellular matrix secretion in the spheroids, which leads to changes in the cell phenotype and secretory profile.

Human MSCs are known for their paracrine secretion of several bioactive molecules that play critical roles in angiogenesis, immunosuppression, cell death, proliferation and cell migration (Boregowda et al. 2018). In addition, MSC growth into

spheroids increases paracrine secretion by these cells, compared with 2D culture (Laschke and Menger 2017). In this study, the analysis of culture supernatants from ASC spheroids revealed that IL-6 secretion increased after 1 day of treatment with AgCl–NPs from *B. megaterium*, in a dose-dependent manner. Furthermore, we observed the highest secretion of IL-6 at day 21 for ASC spheroids treated with 25 μg/mL AgCl–NP from *B. megaterium*. IL-6 alters tissue physiology, mainly through the recruitment of neutrophils and macrophages (Kyurkchiev et al. 2014). Also, IL-6 is one of the main cytokines involved in obesity development, which generates a pro-inflammatory adipose tissue microenvironment (Schmidt et al. 2015).

Although the treatment with AgCl–NPs described here had only minor effects on spheroid morphology and viability, altered levels of IL-6 at day 21 due to the administration of 25 μg/mL AgCl–NPs may lead to disturbances in tissue homeostasis. The increase of IL-6 levels in cells after silver nanoparticles exposure for few days was observed in human lung and human brain cancer cells. The authors proposed that Ag nanoparticles can activate molecular pathways resulting in transcription of genes involved in inflammatory responses (AshaRani et al. 2012). AgCl–NPs from *B. megaterium* influence the secretory profile of ASC, probably due to a continuous activation of molecular pathways involved in inflammatory responses.

IL-8 secretion also increased in the supernatant of ASC spheroids in a dose-dependent manner, at day 1. Interestingly, all groups treated with AgCl-NPs had decreased levels of IL-8 at day 7. IL-8 was reported as being a pro-inflammatory interleukin with pro-angiogenic properties (Hou et al. 2014). Untreated or unstimulated ASC has the capacity to secrete IL-8 (Silva et al. 2015), which contributes to their regenerative capacity (Furuhata et al. 2016). The effects of Ag nanoparticles in cytokines secretion are complex and controversial depending on cell and tissue types (Shin et al. 2007, Nishanth et al. 2011), besides physio- (Hackenberg et al. 2011) and pathological scenarios (Silva et al. 2015). The disparity between IL-6 and IL-8 levels in ASC spheroids treated with 25 μg/mL AgCl–NPs from *B. megaterium* implies that the cytokine secretion of adipose tissue will depend on the dose and time of AgCl-NPs exposure. Our results suggest that alterations in IL-8 secretion may contribute to alter the adipose tissue microenvironment in the early days of exposure to nanoparticles. To the best of our knowledge, there are no studies that evaluate how time in culture affects IL-8 secretion by ASC spheroids treated with nanoparticles.

IL-1β is part of a family of pro-inflammatory cytokines involved in the development of a variety of acute and chronic diseases (Ortiz et al. 2007; Uccelli et al. 2008). IL-1β was not detected at day 1 of treatment with AgCl–NPs, but was detectable in all samples at day 21, while at day 7 of treatment detectable levels of IL-1β were seen only in the group treated with 25 μg/mL AgCl–NPs. At day 21, ASC spheroids treated with 25 μg/mL AgCl–NPs showed the highest secretion compared with all treated groups.

IL-10 is capable of inhibiting the secretion of pro-inflammatory cytokines and chemokines such as IL-6 (Ouyang et al. 2011). The secretion of IL-10 by ASC spheroids at days 7 and 21 may represent an attempt to neutralize the pro-inflammatory cytokine secretion detected from day 1 post-treatment. Curiously, at 21 days of treatment, IL-6 secretion reached a maximum in ASC spheroids treated with 25 μg/mL. Altogether, these results show that AgCl–NP treatment, especially at 25 μg/mL, alters the interleukin profile of the ASC spheroids, indicating that skin implants or products containing AgCl–NPs have the potential to affect the subcutaneous adipose tissue microenvironment.

Transforming growth factor beta (TGF-β) is a pleiotropic cytokine that regulates numerous cellular functions and events such as migration, proliferation, apoptosis, differentiation, immune responses and wound healing (Kyurkchiev et al. 2014). The administration of anti-TGF-β1/2 neutralizing antibody reduces cutaneous scarring in rat incisional wounds (Shah et al. 1995). Moreover, Kryger et al. (2007) reported that high levels of TGF-β1, and possibly TGF-β2, are associated with hypertrophic scar formation in a rabbit model. In light of these reports, we sought to evaluate TGF-β levels in our model, to assess the possibility that AgCl–NPs treatment may disrupt extracellular matrix remodeling in ASCs spheroids. Overall, the secretion of TGF-β1 decreased throughout the treatment period, while TGF-β2 secretion showed a decrease in all treated ASC spheroids at day 1. Further studies are required to exclude a possible effect of AgCl–NPs on extracellular matrix remodeling.

Conclusion

Our results indicate that the sub-lethal concentrations of AgCl–NPs tested here altered the secretory profile of ASC spheroids. Remarkable differences were observed in the dose of 25 μg/mL at early days of treatment for interleukins 6, 8 and 1β. Furthermore, at day 21, ASC spheroids treated with 25 μg/mL AgCl–NPs showed a high level of IL-6 secretion. The maintenance of IL-6 secretion during 21 days of treatment may promote long-term disturbances in adipose tissue homeostasis. Further studies should follow to investigate the effects of AgCl–NPs on the replication of adult stem cells, and on their capacity for tissue repair and differentiation, since the proximity to skin implant surfaces might expose subcutaneous ASCs to AgCl–NPs found in implant coatings and skin products.

Compliance with ethical standards

Conflict of interest   The authors report no conflict of interest.

References

Acharya D, Singha KM, Pandey P, Mohanta B, Rajkumari J, Singha LP (2018) Shape dependent physical mutilation and lethal effects of silver nanoparticles on bacteria. Sci Rep. 8:201. https://doi.org/10.1038/s41598-017-18590-6

Adnan H, Kang I (2015) Preparation of silver nanoparticles and their industrial and biomedical applications: a comprehensive review. Adv Mater Sci Eng. 15:1–16. https://doi.org/10.1155/2015/165257

Alberts C, Hofstetter W, Siebenrock K, Landmann R, Klenke F (2011) In vitro cytotoxicity of silver nanoparticles on osteoblasts and osteoclasts at antibacterial concentrations. Nanotoxicology 7:30–36. https://doi.org/10.3109/17435390.2011.626538

Antony JJ, Sivalingam P, Chen B (2015) Toxicological effects of silver nanoparticles. Environ Toxicol Pharmacol 3:729–732. https://doi.org/10.1016/j.etap.2015.09.003

AshaRani PV, Sethu S, Lim HK, Balaji G, Valiyaveettil S, Hande MP (2012) Differential regulation of intracellular factors mediating cell cycle, DNA repair and inflammation following exposure to silver nanoparticles in human cells. Genome Integr. 3:1–14. https://doi.org/10.1186/2041-9414-3-2

Asl S, Hoaawinpoor H, Parivar K, Roodbari N, Ahvaz H (2017) Physical stimulation and scaffold composition efficiently support osteogenic differentiation of mesenchymal stem cells. Tissue Cell. 50:1–17. https://doi.org/10.1016/j.tice.2017.11.001

Baptista L, Amaral R, Carias R, Aniceto M, Claudio-da-Silva C, Borojevic R (2009) An alternative method for the isolation of mesenchymal stromal cells derived from lipoaspirate samples. Cytotherapy 11:706–715. https://doi.org/10.3109/14653240902981144

Barkat A, Harshita Beg S, Naim J, Potto FH, Singh SP, Ahmad FJ (2017) current progress in synthesis, characterization and applications of silver nanoparticles: precepts and prospects. Recent Pat Anti Infect Drug Discov. 12:1–16. https://doi.org/10.2174/1574891x12666171006102833

Boregowda S, Booker C, Phinney D (2018) Mesenshymal stem cells: the moniker fits the science. Stem Cells 36:7–10. https://doi.org/10.1002/stem.2713

Carlson C, Hussain S, Schrand A, Braydich-Stollen K, Hess K, Jones R, Schlager J (2008) Unique cellular interaction of silver nanoparticles: size-dependent generation of reactive oxygen species. J Phys Chem B 112:13608–13619. https://doi.org/10.1021/jp712087

Chaudhury K, Kumar V, Kandasamy J, RoyChoudhury S (2014) Regenerative nanomedicine: current perspectives and future directions. Int J Nanomed 9:4153–4167. https://doi.org/10.2147/IJN.S45332

Costa M, McDevitt T, Cabral J, Silva C, Ferreira F (2017) Tridimensional configurations of human mesenchymal stem/stromal cells to enhance cell paracrine potential towards wound healing processes. J Biotechnol 262:28–39. https://doi.org/10.1016/j.jbiotec.2017.09.020

Edmondson R, Broglie J, Adcock A, Yang L (2014) Three-dimensional cell culture systems and their applications in drug discovery and cell-based biosensors. Assay Drug Dev Technol 12:207–218. https://doi.org/10.1089/adt.2014.573

Ferreira VS, Ferreira CE, Lima TRM, Frases S, Souza W, Sant'Anna C (2017) Green production of microalgae-based silver chloride nanoparticles with antimicrobial activity against pathogenic bacteria. Enzyme Microb Technol 97:114–121. https://doi.org/10.1016/j.enzmictec.2016.10.018

Furuhata Y, Kikuchi Y, Tomita S, Yoshimoto K (2016) Small spheroids of adipose-derived stem cells with time-dependent enhancement of IL-8 and VEGF-A secretion. Genes Cells 21:1380–1386. https://doi.org/10.1111/gtc.12448

Gopinath P, Gogoi S, Sanpuic P, Paul A, Chattopadhyay A, Ghosh S (2010) Signaling gene cascade in silver nanoparticle induced apoptosis. Colloids Surf B 77:240–245. https://doi.org/10.1016/j.colsurfb.2010.01.033

Hackenberg S, Scherzed A, Kessler M, Hummel S, Technau A, Froelich K, Ginzkey C, Koehler C, Hagen R, Kleinsasser N (2011) Silver nanoparticles: evaluation of DNA damage, toxicity and functional impairment in human mesenchymal stem cells. Toxicol Lett 201:27–33. https://doi.org/10.1016/j.toxlet.2010.12.001

Hou Y, Ryu CH, Jun JA, Kim SM, Jeong CH, Jeun SS (2014) IL-8 enhances the angiogenic potential of human bone marrow mesenchymal stem cells by increasing vascular endothelial growth factor. Cell Biol Int 38:1050–1059. https://doi.org/10.1002/cbin.10294

Hsin Y, Chen C, Huang S, Shih T, Lai P, Chueh P (2008) The apoptotic effect of nanosilver is mediated by a ROS- and JNK dependent mechanism involving the mitochondrial pathway in NIH3T3 cells. Toxicol Lett 179:130–139. https://doi.org/10.1016/j.toxlet.2008.04.015

Jung H, Kim K, Shin S, Kim S, Park Y (2008) Antibacterial activity and mechanism of action of the silver ion in *Staphylococcus aureus* and *Escherichia coli*. Appl Environ Microbiol 74:2171–2178. https://doi.org/10.1128/AEM.02001-07

Kryger Z, Sisco M, Roy N, Lu L, Rosenberg D, Mustoe T (2007) Temporal expression of the transforming growth factor-Beta pathway in the rabbit ear model of wound healing and scarring. J Am Coll Surg 205:78–88. https://doi.org/10.1016/j.jamcollsurg.2007.03.001

Kyurkchiev D, Bochev I, Ivanova-Todorova E, Mourdjeva M, Oreshkova T, Belemezova K, Kyurkchiev S (2014) Secretion of immunoregulatory cytokines by mesenchymal stem cells. World J Stem Cells 6:552–570. https://doi.org/10.4252/wjsc.v6.i5.552

Laschke M, Menger M (2017) Life is 3D: boosting spheroid function for tissue engineering. Trends Biotechnol 35:133–144. https://doi.org/10.1016/j.tibtech.2016.08.004

Lee J, Lilly G, Doty R, Podsiadlo P, Kotov N (2009) In vitro toxicity testing of nanoparticles in 3D cell culture. Small 5:1213–1221. https://doi.org/10.1002/smll.200801788

Luther E, Koehler Y, Diendorf J, Epple M, Dringen R (2011) Accumulation of silver nanoparticles by cultured primary brain astrocytes. Nanotechnology 22:1–12. https://doi.org/10.1088/0957-4484/22/37/375101

Nishanth RP, Jyotsna RG, Schlager JJ, Hussain SM, Reddanna P (2011) Inflammatory responses of RAW 264.7 macrophages upon exposure to nanoparticles: role of ROS-NFkappaB signaling. Nanotoxicology. 5:502–516. https://doi.org/10.3109/17435390.2010.541604

Ortiz L, DuTreil M, Fattman C, Pandey A, Torres G, Go C, Phinney D (2007) Interleukin 1 receptor antagonist mediates the antiinflammatory and antifibrotic effect of mesenchymal stem cells during lung injury. Proc Natl Acad Sci USA 104:11002–11007. https://doi.org/10.1073/pnas.0704421104

Ouyang W, Rutz S, Crellin N, Valdez P, Hymowitz S (2011) Regulation and fuctions of the IL-10 family of cytokines in inflammation and disease. Annu Rev Immunol 29:71–109. https://doi.org/10.1146/annurev-immunol-031210-101312

Park E, Yi J, Kim Y, Choi K, Park K (2010) Silver nanoparticles induce cytotoxicity by a Trojan-horse type mechanism. Toxicol In Vitro 24:872–878. https://doi.org/10.1016/j.tiv.2009.12.001

Pascarelli A, Moretti E, Terzuoli G, Lamboglia A, Renieri T, Fioravanti A, Collodel G (2013) Effects of gold and silver nanoparticles in cultured human osteoarthritic chondrocytes. J Appl Toxicol 33:1506–1513. https://doi.org/10.1002/jat.2912

Qin H, Zhu C, An Z, Jiang Y, Zhao Y, Wang J, Liu X, Hui B, Zhang X, Wang Y (2014) Silver nanoparticles promote osteogenic differentiation of human urine-derived stem cells at noncytotoxic concentrations. Int J Nanomed 9:2469–2478. https://doi.org/10.2147/IJN.S59753

Samberg M, Oldenburg S, Nancy A, Riviere N (2010) Evaluation of silver nanoparticle toxicity in skin in vivo and keratinocytes in vitro. Environ Health Perspect 118:407–413. https://doi.org/10.1289/ehp.0901398

Sart S, Tsai C, Li Y, Ma T (2014) Three-dimensional aggregates of mesenchymal stem cells: cellular mechanisms, biological properties and applications. Tissue Eng Part B Rev 20:365–380. https://doi.org/10.1089/ten.TEB.2013.0537

Schmidt F, Weschenfelder J, Sander C, Minkwitz J, Thormann J, Chittka T, Mergl R, Kirkby K, Fabahauer M, Stumvoll M, Holdt L, Teupser D, Hegerl U, Himmerich H (2015) Inflammatory cytokines in general and central obesity and modulating effects of physical activity. PLoS ONE 10:1–17. https://doi.org/10.1371/journal.pone.0121971

Shah M, Foreman D, Ferguson M (1995) Neutralisation of TGF-beta 1 and TGF-beta 2 or exogenous addition of TGF-beta 3 to cutaneous rat wounds reduces scarring. J Cell Sci 108:985–1002

Shin SH, Ye MK, Kim HS, Kang HS (2007) The effects of nano-silver on the proliferation and cytokine expression by peripheral blood mononuclear cells. Int Immunopharmacol. 7:1813–1818. https://doi.org/10.1016/j.intimp.2007.08.025

Silva KR, Liechocki S, Carneiro JR, Claudio-da-Silva C, Maya-Monteiro CM, Borojevic R, Baptista LS (2015) Stromal-vascular fraction content and adipose stem cell behavior are altered in morbid obese and post bariatric surgery ex-obese women. Stem Cell Res Therapy. 6:1–13. https://doi.org/10.1186/s13287-015-0029-x

Srikar SK, Giri DD, Pal DB, Mishra PK, Upadhyay SN (2016) Green synthesis of silver nanoparticles: a review. Green Sustain Chem 6:34–36. https://doi.org/10.4236/gsc.2016.61004

Stolle L, Hussain S, Schlager J, Hofmann C (2005) In vitro cytotoxicity of nanoparticles in mammalian germline stem cells. Toxicol Sci 88:412–419. https://doi.org/10.1093/toxsci/kfi256

Stuart MP, Matsui RA, Santos MFS, Cortes I, Azevedo MS, Silva KR, Beatrici A, Leite PE, Falagan P, Granjeiro JM, Mironov V, Baptista LS (2017) Successful low-cost scaffold-free cartilage tissue engineering using human cartilage progenitor cell spheroids formed by micromolded nonadhesive hydrogel. Stem Cells Int (online). 17:1–11. https://doi.org/10.1155/2017/7053465

Taylor U, Tiedemann D, Rehbock C, Kues WA, Barcikowski S, Rath D (2015) Influence of gold, silver and gold–silver alloy nanoparticles on germ cell function and embryo development. Beilstein J Nanotechnol 6:651–664. https://doi.org/10.3762/bjnano.6.66

Tormos KV, Anso E, Hamanka RB, Eisenbart J, Joseph J, Kalyanaraman B, Chandel NS (2011) Mitochondrial complex III ROS regulate adipocyte differentiation. Cell Metab 14:537–544. https://doi.org/10.1016/j.cmet.2011.08.007

Tripathi DK, Tripathi A, Shweta Singh S, Singh Y, Vishwakarma K, Yadav G, Sharma S, Singh VK, Mishra RK, Upadhyay RG, Dubey NK, Lee Y, Chauhan DK (2017) Uptake, accumulation and toxicity of silver nanoparticle in

autotrophic plants, and heterotrophic microbes: a concentric review. Front Microbiol 8:1–7. https://doi.org/10.3389/fmicb.2017.00007

Uccelli A, Moretta L, Pistoia V (2008) Mesenchymal stem cells in health and disease. Nat Rev Immunol 8:726–736. https://doi.org/10.1038/nri2395

Wang X, Chang H, Francis R, Olszowy H, Liu P, Kempf M, Cuttle L, Kravchuk O, Phillips G, Kimble R (2009) Silver deposits in cutaneous burn scar tissue is a common phenomenon following application of a silver dressing. J Cutan Pathol 36:788–792. https://doi.org/10.1111/j.1600-0560.2008.01141.x

Wang J, Li J, Guo G, Wang Q, Tang J, Zhao Y, Qin H, Wahafu T, Shen H, Liu X, Zhang X (2016) Silver-nanoparticles-modified biomaterial surface resistant to staphylococcus: new insight into the antimicrobial action of silver. Sci Rep 6:1–16. https://doi.org/10.1038/srep32699

Waters R, Alam P, Pacelli S, Chakravarti A, Ahmed R, Paul A (2017) Stem cell-inspired secretome-rich injectable hydrogel to repair injured cardiac tissue. Acta Biomater. 15:95–106. https://doi.org/10.1016/j.actbio.2017.12.025

Wijnhoven S, Peijnenburg W, Herberts C, Hagens W, Oomen A, Heugens E, Roszek B, Bisschops J, Gosens I, Meent D, Dekkers S, Jong W, Zijverden M, Sips A, Geertsma R (2009) Nano-silver—a review of available data and knowledge gaps in human and environmental risk assessment. Nanotoxicology 3:109–138. https://doi.org/10.1080/17435390902725914

Zhang Y, Marsboom G, Toth PT, Rehman J (2013) Mitochondrial respiration regulates adipogenic differentiation of human mesenchymal stem cells. PLoS ONE. 8:1–12. https://doi.org/10.1371/journal.pone.0077077

Zhang X, Shen W, Gurunathan S (2016a) Silver nanoparticle-mediated cellular responses in various cell lines: an in vitro model. Int J Mol Sci 17:1–26. https://doi.org/10.3390/ijms17101603

Zhang XF, Liu ZG, Shen W, Gurunathan S (2016b) Silver nanoparticles: synthesis, characterization, properties, applications, and therapeutic approaches. Int J Mol Sci 17:1–34. https://doi.org/10.3390/ijms17091534